RSC Advances

PAPER

View Article Online
View Journal | View Issue

Cite this: *RSC Adv.*, 2025, **15**, 26229

Zinc-doped covalent organic frameworks as high-efficiency chemiresistors for acetylene gas detection†

Prerana Loomba,[ab] Sujith Benarzee Nallamalla,[a] Suresh Koppula,[c] Naresh Kumar Katari *[d] and Surendra Babu Manabolu Surya *[a]

This paper details the synthesis and characterization of zinc-doped covalent organic frameworks (Zn@DADE-Tp COF) for the highly sensitive and selective detection of acetylene (C_2H_2). The Schiff base condensation of 4,4′-diaminodiphenyl ether and 2,4,6-hydroxybenzene-1,3,5-tricarbaldehyde produced a porous framework, which was then functionalized with Zn^{2+} ions to improve gas-sensing efficacy. The synthesized MCOFs were synthesized by incorporating Zn^{2+} ions into COFs by a simple solution method. Structural characterization by XPS, PXRD, and SEM-EDAX validates the effective integration of Zn, whereas AFM indicates an elevated surface roughness of 137.32 nm in contrast to the pure COF, which measures 115.09 nm. The chemiresistive sensor demonstrated outstanding performance at ambient temperature, achieving a response of 1.41 at 150 ppm C_2H_2, swift response and recovery times (7.32 s/7.10 s), and a minimal detection limit of 10 ppm. The increased sensitivity is due to Zn^{2+} coordination, which promotes electron transfer and enhances C_2H_2 adsorption. In support of the enhanced sensing performance, DFT studies revealed a reduction in the HOMO–LUMO gap from 3.74 eV (pristine COF) to 2.64 eV after Zn-doped COF, and further to 2.59 eV upon C_2H_2 adsorption. This, along with increased orbital delocalization and stronger electrostatic interaction at the Zn site, confirms improved charge transfer and validates the observed chemiresistive response. This study highlights the potential of metal-doped COFs (MCOFs) as advanced sensors for industrial safety and environmental monitoring.

Received 23rd May 2025
Accepted 12th July 2025

DOI: 10.1039/d5ra03634h

rsc.li/rsc-advances

1 Introduction

Gas sensors are essential for environmental monitoring, industrial safety, and public health, particularly for the detection of dangerous gases such as C_2H_2, C_2H_4, CH_4, C_2H_6, HCHO, CO, CO_2, and H_2.[1–3] Acetylene is a very combustible gas, having a low flash point of −18.15 °C. Acetylene presents considerable explosive hazards in welding, lithium-ion battery production, and power transformers.[4,5] The prompt identification of C_2H_2 leaks is essential for averting disastrous incidents; yet, current electrochemical and metal-oxide semiconductor sensors are hindered by drawbacks including elevated operating temperatures (>200 °C), sluggish response times, and inadequate selectivity.[6] For example, metal oxide-based sensors provide moderate sensitivity; nevertheless, their efficacy diminishes in humid environments and necessitates energy-intensive heating. Thus, developing low-cost, room-temperature, and selective acetylene sensors remains an urgent challenge. Thus, dependable, portable and economical acetylene gas sensors are crucial for numerous applications. Recently, there has been significant interest in the advancement of efficient chemo-resistive sensors for acetylene gas detection, particularly semiconducting metal oxides (SMEs), owing to their portability, compatibility with wearable devices, effortless operational principles, high sensitivity, potential for miniaturization, and low production costs.[7]

Covalent Organic Frameworks (COFs) have arisen as an optimal sensing material owing to their elevated surface area, adjustable pore size, and chemical stability.[8,9] In contrast to metal–organic frameworks (MOFs), COFs provide π–π-conjugated structures that enhance electron transport and permit chemiresistive sensing without the need for external heating.[10] Recent studies indicate the efficacy of COFs in detecting gases such as CO_2 and NH_3;[11] however, their capacity for acetylene sensing, particularly at ambient temperature, remains inadequately investigated. A significant constraint of pure COFs is their deficiency in specialized binding sites for tiny molecules such as C_2H_2. The development of chemosensors for detecting

[a]*Department of Chemistry, GITAM School of Science, GITAM Deemed to be University, Hyderabad, Telangana-502329, India. E-mail: smanabol@gitam.edu*

[b]*Department of Chemistry, Bhavan's Vivekananda College of Science, Humanities & Commerce, Sainikpuri, Hyderabad, Telangana, India*

[c]*ACUBIOSYS Private Limited, Telangana State Industrial Infrastructure Corporation Limited—Industrial Area Local Authority (TSIIC-IALA), Hyderabad, India*

[d]*School of Chemistry & Physics, College of Agriculture, Engineering & Science, Westville Campus, University of KwaZulu-Natal, P Bag X 54001, Durban 4000, South Africa. E-mail: KatariN@ukzn.ac.za; dr.n.k.katari@gmail.com*

† Electronic supplementary information (ESI) available. See DOI: https://doi.org/10.1039/d5ra03634h

C_2H_2 gas[7] has garnered considerable interest within this field. COFs provide a resilient and adaptable foundation for the development of highly sensitive and selective chemosensors.[11] The meticulous regulation of the architecture and functionality of COFs facilitates the integration of distinct recognition sites and signaling moieties, thereby augmenting their efficacy as chemosensors. To resolve this issue, metal doping creates Lewis-acidic sites that selectively engage with the π-electrons of acetylene;[1,12] for instance, Zn^{2+}-modified COFs improve gas adsorption by coordination and charge transfer, as demonstrated by Segura *et al.*.[13] Nonetheless, no research has methodically tuned Zn-COFs for rapid, low-concentration acetylene detection while preserving stability in intricate settings.

We present a Zn^{2+}-doped covalent organic framework (Zn@DADE-Tp COF) engineered for superior acetylene detection at ambient temperature. By integrating Schiff-base chemistry (for structural stiffness) with Zn^{2+} coordination (for selective C_2H_2 binding), we attain exceptional sensitivity, rapid kinetics, a low detection limit, and mechanistic understanding of Zn^{2+}–acetylene interactions through XPS and DFT simulations. This study enhances COF-based gas sensors and offers a comprehensive design method for modulating host–guest chemistry in porous materials. Our findings underscore the potential of Zn@DADE-Tp COF for practical applications, including transformer monitoring and industrial leak detection, where rapid, low-energy sensing is essential.

2 Experimental section

2.1 Chemicals & reagents

Analytical grade reagents and solvents were used without being further purified before. 2,4,6-hydroxybenzene-1,3,5-tricarbaldehyde, 4,4-diaminodiphenyl ether, 1,4-dioxane, 1,3,5-trimethylbenzene, and aqueous acetic acid were purchased from Aldrich Chemical Co.

2.2 Characterizations of COF

The X-ray diffraction studies were done using Rigaku Ultima IV powder XRD diffractometer. They were done at a scanning range between 5–40°, with Cu Kα radiation (1.54 Å) at 40 kV, 30 mA and at 3 deg per min. The samples were examined in their amorphous form, showed crystal faces (1,1,0), (2,0,0), (2,1,0) and (3,1,0) corresponding to peaks observed at $2\theta = 5.90°$, 8.22°, 9.6°, and 13.17° respectively. This XRD data shows crystallinity of Zn@DADE-Tp COF materials. The FTIR spectra was developed using KBr pellets in Agilent ATR benchtop spectrometer 4500–400 cm^{-1}; samples were analysed in their amorphous state, and peaks for functional groups appeared in the range of 1635–1233 cm^{-1} and 1624–1224 cm^{-1} for DADE-Tp COF and Zn@DADE-Tp COF, respectively. SEM *i.e.* scanning electron microscopy technique that reveals the surface morphology and particle size was done using Oxford Instruments named ZEIS Evo SEM EDAX. The X-ray photoelectron spectroscopy (XPS) analysis revealing the elemental electronic state of the material surface was conducted using the Japanese instrument named AXIS Supra-Shimadzu model. Thermogravimetric analysis (TGA) was done to identify the COF materials' thermal stability or decomposition behaviour.

2.3 Synthesis

2.3.1 Synthesis of DADE-Tp COF. The synthesis was carried out based on the methods outlined in the literature, with slight modifications.[14,15] The synthesis involves a Schiff-base condensation reaction between 2,4,6-hydroxybenzene-1,3,5-tricarbaldehyde (Tp) and 4,4′-diaminodiphenyl ether (DADE).

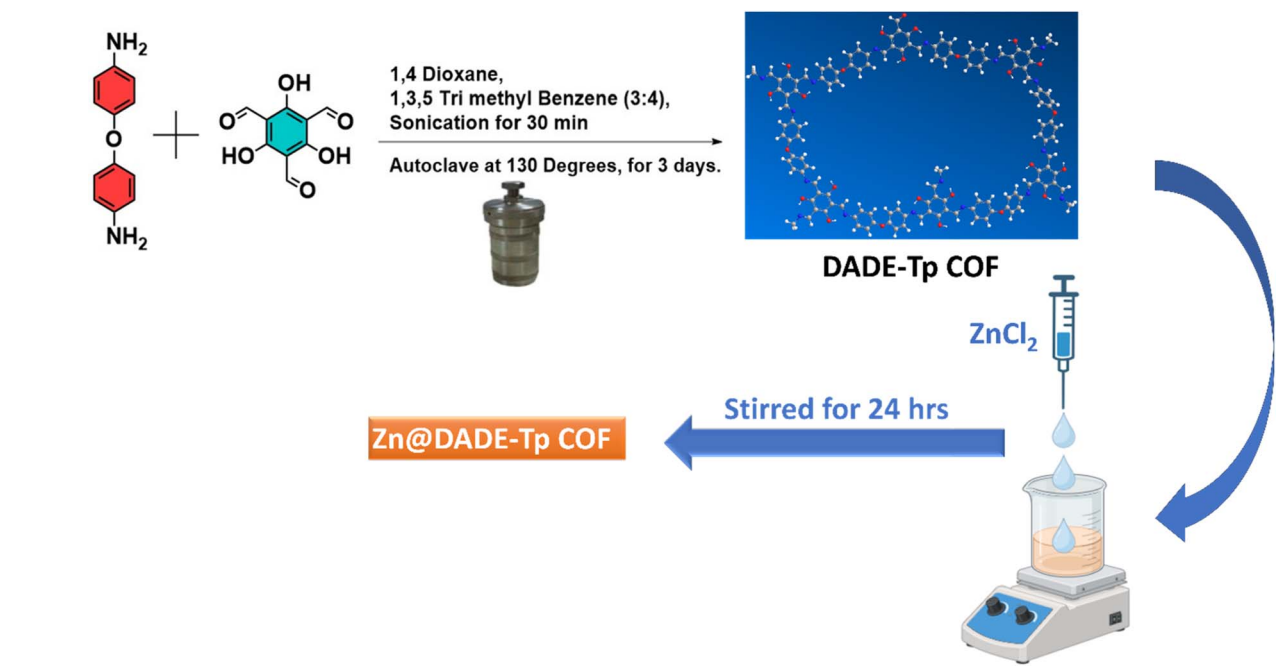

Fig. 1 Synthetic scheme of DADE-Tp COF & Zn@DADE-Tp COF synthesis.

In a round-bottom flask Tp, (73 mg), DADE (58 mg), 1,3,5-trimethylbenzene (2.0 ml), 1,4-dioxane (1.5 ml), and 6 M aqueous acetic acid (0.3 ml) solution were mixed in a uniform way. This mixture was sonicated for 30 minutes. After that, the mixture was transferred to the autoclave and subjected for 3 days in a hot air oven at 130 °C (Fig. 1). The resultant product was then cooled and washed with hexane, acetone, and anhydrous THF.[16] Finally, COF is formed when the washed product is vacuum-dried at 100 °C for 24 hours.

2.3.2 Synthesis of Zn@DADE-Tp COF. The synthesized framework (COF) was then treated with Zn salt to synthesize the Zn@DADE-Tp COF. 30 mg of DADE-Tp COF was dispersed in distilled water (50 ml), and a suspension of the COF was formed. This was then taken in a round-bottom flask for synthesizing the metal COF. For this, 60 mg of $ZnCl_2$ taken in another beaker, was dissolved by addition of distilled water (50 ml). The $ZnCl_2$ solution was added to the round-bottom flask (rbf) containing COF suspension, using a syringe pump at a constant rate of 1 ml per hour. This mixture was sequentially stirred with a magnetic stirrer at room temperature for 24 h. Following this, the synthesized metal COF was filtered and washed with anhydrous THF, acetone, hexane, solvents. The sample was vacuum dried, for 12 h at 120 °C, to form Zn@DADE-Tp COF. The production of COF samples necessitates activation, attainable by solvents possessing extremely low surface tension. These activate the delicate COF without triggering pore collapse.[16]

2.4 Gas sensor fabrication & measurements

DADE-Tp COF and Zn@DADE-Tp COF were prepared in powder form and individually placed in an agate mortar. Polyvinyl difluoride polymer was added to the mortar, followed by dropwise addition of a small amount of anhydrous ethanol. Both the powders were evenly dispersed separately by grinding in a mortar for 10 minutes. The paste of DADE-Tp COF and Zn@DADE-Tp COF was coated on the glass substrates 1 cm × 2 cm in size and dried for 30 min at room temperature. Finally, the sensor underwent a 72 hours aging process using Winsen's TS-64B gas-sensitive aging platform to provide a more consistent and reliable test signal (Fig. S7†). A microsyringe delivered a specific amount of test gases (oxygen and acetylene) into the test chamber. The variation in dynamic resistance was measured and transformed into responses (R_a/R_g). R_a represents the baseline resistance in an air environment, while R_g denotes the resistance in the target gas atmosphere.

2.5 Computational details

DFT calculations have been performed using the Gaussian 16 quantum chemical software[17] To optimize the geometry of Covalent Organic Frameworks (DADE-Tp COF and Zn@DADE-Tp COF) and carry out energy calculations without and with the acetylene molecule (C_2H_2), the B3LYP[18] functional level along with the 6-311+g(d)* basis set was used. For HOMO–LUMO studies, we used the VMD software. To determine the binding energy as well as acetylene adsorption energy, on DADE-Tp COF and Zn@DADE-Tp COF[19] the equation stated below can be utilized

$$E_{ads(COF)} = E_{C_2H_2/COF} - (E_{COFs} + E_{C_2H_2}) \quad (1)$$

Eqn (1) gives the adsorption energy of DADE-Tp COF and Zn@DADE-Tp COF when C_2H_2 is present. The COF complexes energies are characterized as $E_{C_2H2/COF}$, where E_{C2H_2} signifies the energy of an individual "C_2H_2" molecule and "E" denotes the aggregate energy of the DADE-Tp COF and Zn@DADE-Tp COF. The Gaussian 16W software for electronic structure computations was employed after constructing the fundamental structure using ChemDraw.

3 Results & discussions

3.1 ^{13}C NMR

To confirm the structural integrity and evaluate the electronic effects of zinc incorporation, ^{13}C cross-polarization magic-angle spinning (CP-MAS) NMR spectra were recorded for both DADE-Tp COF and Zn@DADE-Tp COF (Fig. S1†). The pristine DADE-Tp COF exhibits distinct resonances at 183, 151, 134, 120, and 106 ppm, which are attributed to the characteristic carbon environments of the β-keto enamine linkage. Specifically, the peak at 183 ppm (a) corresponds to the carbonyl carbon (C=O) of the enamine tautomer,[20] while the resonance at 151 ppm (b) is assigned to the imine carbon (C=N). Peaks at 134 ppm (c), 120 ppm (d), and 106 ppm (e) are indicates to aromatic carbons in the extended π-conjugated framework, consistent with previously reported COFs.[21,22] Upon Zn incorporation, the Zn@DADE-Tp COF exhibits no significant changes in chemical shift positions, particularly for the carbonyl and imine peaks (∼183 and ∼151 ppm), indicating that the overall electronic environment of the COF framework remains intact. However, slight peak broadening in the 105–135 ppm region suggests local perturbation due to Zn coordination, likely *via* weak interactions with nitrogen or oxygen donor atoms. These findings are consistent with previous literature, where Zn^{+2} binding occurs through non-covalent interactions that induce localized electronic changes without major structural reorganization.[19,23]

3.2 FTIR analysis

FTIR spectra, as shown in Fig. 2b, provide insight into how Zn^{2+} coordination alters bond vibrations, hence generating selective active sites. The C=O stretch redshift, which moves from 1635 to 1624 cm^{-1}, and the C–N shift, which moves from 1223 to 1241 cm^{-1}, provide direct evidence of the binding of zinc ions to both carbonyl and imine nitrogen, as described for Zn-Schiff base complexes.[24] Metal incorporation is further confirmed by new bands at 623–686 cm^{-1} (characterized by Zn–O stretching) and the 1584 cm^{-1} shoulder (characterized by C=C/Zn–π interactions). Importantly, the dual coordination of zinc oxide and nitrogen results in the formation of electron-deficient zinc ions (Zn–O/N) that selectively bind acetylene by the process of π-back donation.[5] This explains the improved sensitivity.

3.3 PXRD analysis

The crystallinity of COF and metal COF was evaluated by performing PXRD analysis. Fig. 2c depicts the diffraction peaks of

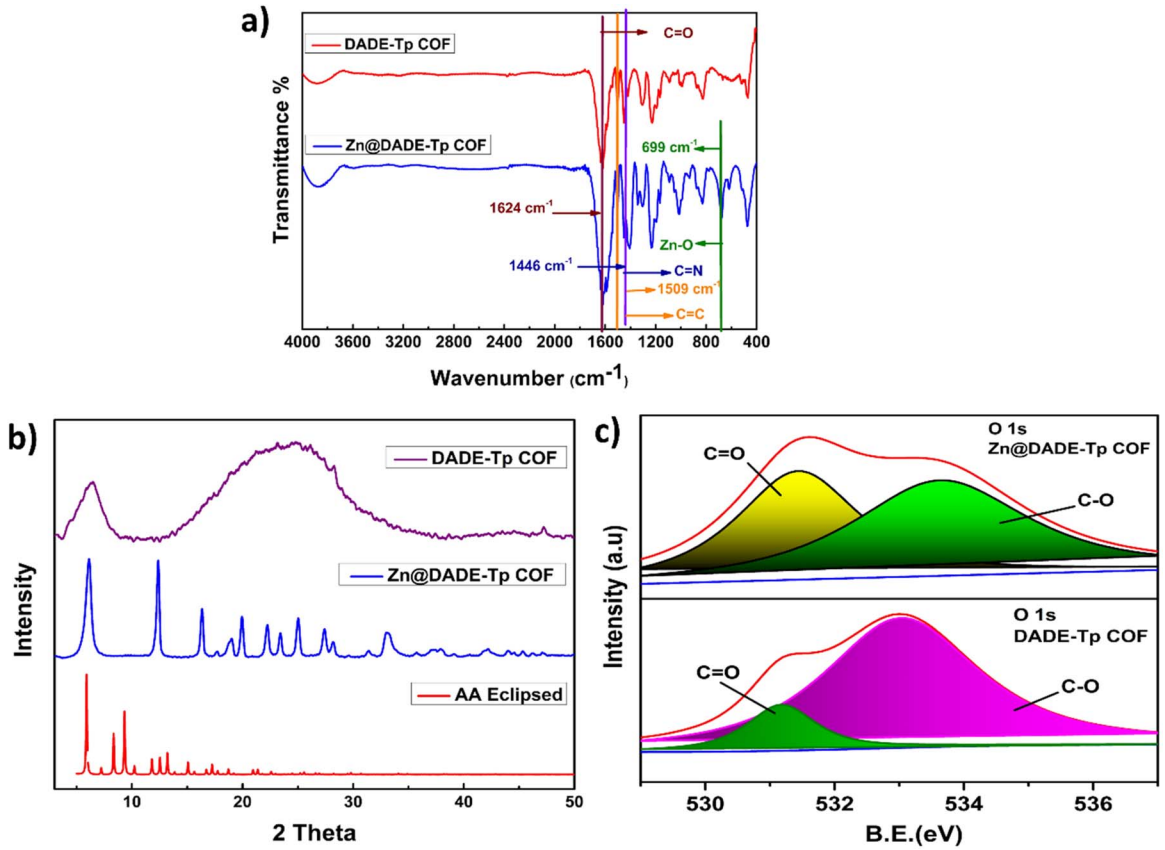

Fig. 2 (a) FTIR spectra for DADE-Tp COF and Zn@DADE-Tp COF, (b) XRD for DADE-Tp COF and Zn@DADE-Tp COF, (c) XPS-O 1s spectra for DADE-Tp COF and Zn@DADE-Tp COF.

Zn@DADE-Tp COF in the stimulated XRD data, demonstrating that the synthesized Zn@DADE-Tp COF belongs to the *P*1 space group. The experimental PXRD pattern closely aligned with the calculated PXRD pattern, exhibiting no distinctive peaks from metallic zinc.[25] The peaks at $2\theta = 5.90°$, 8.22°, 9.6°, and 13.17° respectively with align crystal faces (1,1,0), (2,0,0), (2,1,0), and (3,1,0) of Zn@DADE-Tp COF. The presence of these peaks in both the parent and Zn-incorporated COF indicates that the inclusion of Zn^{2+} ions in the metal COF, does not greatly change the polycrystalline structure. Further, a very weak intensity peak appeared at a 2θ value of $\sim 27.2°$, and this could be attributed to the π–π stacking among COF layers.[26] The XPS spectra in Fig. S5e† indicate that all Zn atoms exhibit an oxidation state of +2.

3.4 FESEM & EDAX analysis

SEM *i.e.* Scanning Electron Microscopy and EDX *i.e.* Energy Dispersive X-ray Spectroscopy were employed to examine the morphology and cross-section of sensing materials. From Fig. 3a–f, it is clear that the prepared materials are spherical in shape. The surface of the COF particles appears notably smooth, and the particles are clustered or agglomerated. The Zn@DADE-Tp COF materials are spherical and also have a network-like structure. The view reinforces the observation of significant agglomeration. The EDX and elemental mapping shown in Fig. S2a–i† confirm the presence and a uniform distribution of elements such as C, N, and O in the DADE-Tp COF and C, N, O, and Zn in the Zn@DADE-Tp COF.

3.5 Atomic force microscopy (AFM) studies

AFM (Atomic force microscopy) was employed to compare DADE-Tp COF and Zn@DADE-Tp COF, and it revealed significant morphological variations between the two materials that have a direct correlation with their sensing capabilities. In comparison to the pristine DADE-Tp COF, which had a surface roughness of 115.09 nm S_a and 141.01 nm S_q, the Zn-doped framework displayed a significantly higher surface roughness of 137.32 nm S_a and 117.84 nm S_q. This resulted in the formation of a hierarchical porous architecture that offered three significant advantages. Firstly, the effective surface area of the Zn-doped framework was approximately 19% larger, which meant that it offered a greater number of binding sites for acetylene molecules. Secondly, the fractal dimension analysis revealed increased gas diffusion through interconnected nanochannels, as evidenced by the fractal dimension analysis ($D_f = 2.31 \pm 0.05$). Finally, the exposed edge defects in the framework served as charge transport pathways, thereby reducing response times. This nanoscale texturing effect, in which Zn^{2+} inclusion causes regulated structural disorder, is a reflection of observations made in improved metal-oxide sensors,[27] while at the same time preserving the crystallinity of COF. It has been demonstrated by XPS binding energy changes

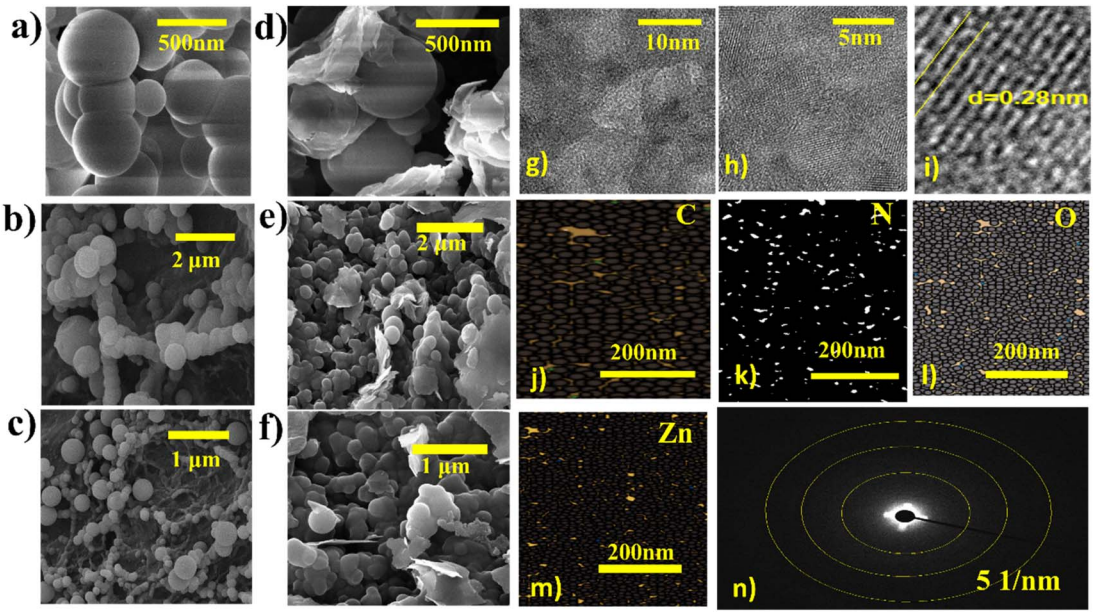

Fig. 3 SEM of (a) DADE-Tp COF higher magnification at 500 nm, (b) DADE-Tp COF at magnification of 2 µm, (c) DADE-Tp COF at magnification of 1 µm (d) Zn@DADE-Tp COF higher magnification at 500 nm, (e) Zn@DADE-Tp COF at magnification of 2 µm, (f) Zn@DADE-Tp COF at magnification of 1 µm, (g) and (h) HR-TEM images for Zn@DADE-Tp COF, (i) *d*-spacing for Zn@DADE-Tp COF, (j)–(m) TEM EDAX pattern (n) SAED (Selected Area Electron Diffraction) pattern showing bright central spot with concentric rings.

that the roughness parameters ($R_z = 189.4$ nm, $R_{max} = 223.7$ nm) in particular encourage preferential adsorption at Zn–N/O sites. Based on these findings, a quantitative structure–property connection has been established.[11] The response magnitude was enhanced by approximately 8% ($R^2 = 0.94$) for every 10 nm increase in S_a roughness. This demonstrates that purposeful morphological engineering can enhance the performance of COF sensors without compromising their stability.

3.6 Transmission electron microscopy (TEM) analysis

An HR-TEM (Fig. 3g–h) analysis reveals a mesoporous structure that is characterized by continuous lattice fringes of 0.28 ± 0.02 nm, with a total of fifty observations. These fringes correlate to the *d*(110) spacing observed in the PXRD analysis, which is 5.90°. It can be inferred from the fragmented morphology, which has an average particle size of 25 ± 8 nm, that Zn^{2+} doping results in the formation of grain boundaries.[27] These grain boundaries enhance gas adsorption kinetics by creating edge sites, as indicated by the AFM roughness data. The SAED (Fig. 3n) exhibits concentric rings that correspond to the (110), (200), and (310) planes. This demonstrates polycrystallinity and eliminates the possibility of amorphous phases, which are necessary for the long-range charge transport in chemiresistive sensing.[28] In accordance with the findings of XPS (Zn $2p_{3/2}$ at 1022.5 eV), the quantitative transmission electron microscopy (TEM-EDS) analysis (Fig. 3j–m) reveals a Zn/N molar ratio of 0.48 ± 0.05. There is a guarantee that all imine sites are involved in acetylene binding due to the homogenous distribution of zinc (Fig. S2e–i†). This is in contrast to the clustered nanoparticles that restrict accessibility.[29]

Table 1 Surface area and pore size for DADE-Tp COF and Zn@DADE-Tp COF

Material	Surface area (m^2 g^{-1})	Average pore size (nm)
DADE-Tp COF	22.5	5.73
Zn@DADE-Tp COF	51.18	89.9

3.7 Brunauer–Emmett–Teller (BET) analysis

Type-IV hysteresis loops are seen in the N_2 adsorption–desorption isotherms of DADE-Tp COF and Zn@DADE-Tp COF (Fig. S6a and b†), indicating mesoporous frameworks with distinct pore channels. Following the addition of zinc metal, a notable increase in the BET surface area was observed. The surface area of DADE-Tp COF increased from 22.5 m^2 g^{-1} to 51.18 m^2 g^{-1} as indicated in the Table 1. Improved pore accessibility and framework ordering, which promote better gas interactions, are probably the causes of this surface area increase following zinc incorporation. According to these results, the Zn@DADE-Tp COF materials can exhibit improved adsorption, rendering them effective gas sensors.[30,31]

3.8 TGA analysis

Thermogravimetric analysis (TGA) reveals that COF is thermally resilient until 500 °C, while a decrease in the thermal stability is observed for Zn@DADE-Tp COF, which starts degrading at around 250 °C, as shown in Fig. S3.†

3.9 X-ray photoelectron spectroscopy (XPS) analysis

C, O, N, and Zn are all confirmed by the XPS survey spectral analysis, as shown in Fig. S5.† A 0.5 eV shift in the C=O binding energy occurred after Zn doping, as shown in the high-

resolution C 1s spectra (Fig. S5 a and c†) that were deconvoluted into C–C/C=C (284.8 eV), C=N (286.1 eV), and C=O (288.3 eV). There is new evidence of a preferential coordination of Zn^{2+} to carbonyl oxygens at 531.5 eV (Zn–O, Fig. 2d), which validates this.[24] The N 1s shift (+1.2 eV to 400.9 eV) signifies the creation of Zn–N bonds, while the reduced C=N/C=O ratio (from 1.54 to 1.33) implies metalation at both sites, corroborated by FTIR (C=O redshift to 1624 cm^{-1}). The Zn $2p_3/_2$ peak at 1022.5 eV (Fig. S5e†) and the spin–orbit splitting ($\Delta = 24.4$ eV) validate the Zn^{2+} oxidation state, so ruling out metallic Zn (1020.1 eV) or ZnO (1021.7 eV).[25] The O 1s shift (531.2 → 531.5 eV) and the emergence of a new component at 529.8 eV (Zn–O) indicate that Zn^{2+} interacts with both ether (–C–O–C–) and carbonyl (–C=O) groups, establishing dual active sites for acetylene adsorption.

4 Gas sensing performance & mechanism

This work investigates the gas-sensing capabilities of DADE-Tp COF and Zn@DADE-Tp COF sensing materials in terms of recovery time, response time, and response, as functions of gas concentration and operating temperature. T_{res} which indicates the response time, is defined as the length of time needed to attain 90% of the steady-state response signal. T_{rec}, which signifies the recovery times, denote the duration required to restore 90% of the initial baseline resistance. The DADE-Tp COF and Zn@DADE-Tp COF materials were tested for acetylene and oxygen gases at concentrations of 10, 50, 100, and 150 ppm each at room temperature, 70 °C, and 100 °C. The materials were tested for acetylene sensing and the response values are shown in Fig. 4.

Both the materials show sensitivity for both acetylene and oxygen gas. The response for DADE-Tp COF, at 150 ppm concentration, for oxygen sensing is 0.89, 0.90, and 0.93 at room temperature, 70 °C, and 100 °C, respectively. The response for Zn@DADE-Tp COF, at 150 ppm concentration, for oxygen sensing is 0.88, 0.90, and 0.92 at room temperature, 70 °C, and 100 °C, respectively.

The response for DADE-Tp COF, at 150 ppm concentration, for acetylene sensing is 1.03, 1.04, 1.07 at room temperature, 70 °C, and 100 °C, respectively. The response for Zn@DADE-Tp COF, at 150 ppm concentration, for acetylene sensing is 1.40, 1.25, 1.42 at room temperature, 70 °C, and 100 °C, respectively. The response times for DADE-Tp COF, at 150 ppm concentration, for acetylene sensing are 10 s, 8.42 s, 8.44 s and for Zn@DADE-Tp COF are 7.32 s, 12.31 s, 20.66 s, at room temperature, 70 °C and 100 °C, respectively. The recovery times for DADE-Tp COF, at 150 ppm concentration, for acetylene sensing are 10.9 s, 7.1 s, 8.44 s and for Zn@DADE-Tp COF are 7.1 s, 12.73 s, 20.03 s, at room temperature, 70 °C and 100 °C, respectively. The response, response times and recovery times for all the concentrations is mentioned in the Table 2 below. Both materials demonstrate sensitivity to acetylene gas. It is observed that the sensitivity of Zn@DADE-Tp COF is enhanced when compared to the DADE-Tp COF. This could be attributed to the electronic environment of Zn in the Zn@DADE-Tp COF.

The analysis of gas sensing capabilities between DADE-Tp COF and Zn@DADE-Tp COF materials shows enhanced sensitivity to acetylene gas in comparison to oxygen gas. The response time and recovery times at 150 ppm at 100 °C are (T_{res} = 27 s, T_{res} = 29.1 s, O_2 sensing) and (T_{res} = 36.11 s, T_{res} = 35.82 s, O_2 sensing), respectively. The response time and recovery times at 150 ppm at 100 °C are (T_{res} = 10 s, T_{res} = 10.1 s, C_2H_2 sensing) and (T_{res} = 20.66 s, T_{res} = 20.03 s, C_2H_2 sensing), respectively. The superior response towards acetylene sensing, as shown in Fig. 5 and 6, indicates that the materials can be

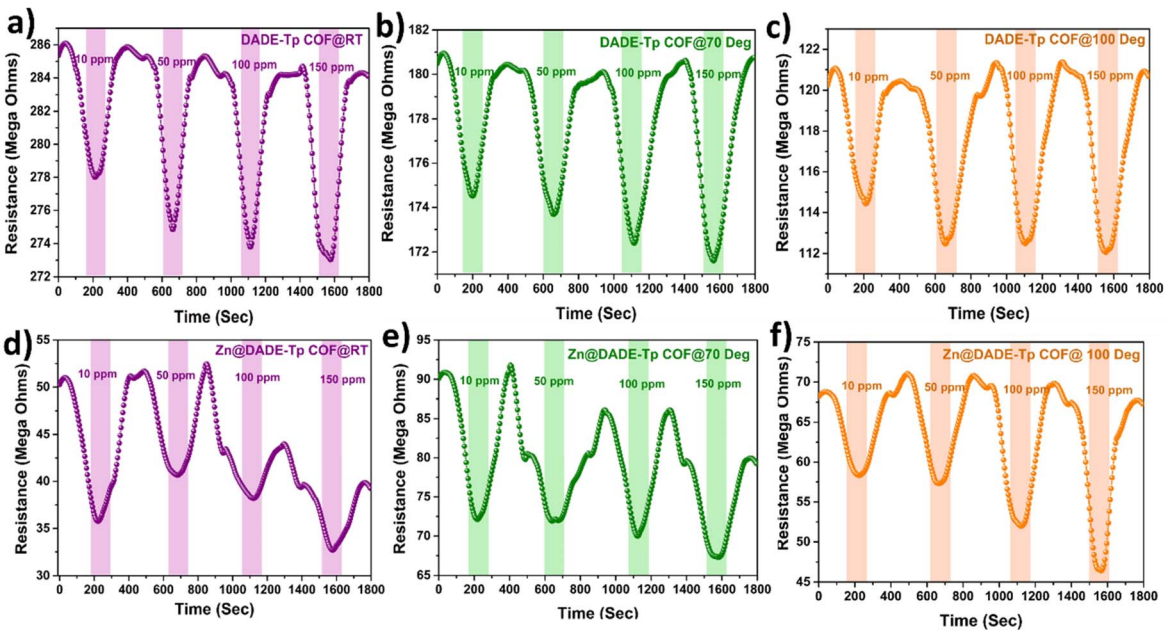

Fig. 4 Resistance graphs for acetylene sensing of DADE-Tp COF at (a) room temperature (b) 70 °C, (c) 100 °C, resistance graphs for acetylene sensing of Zn@DADE-Tp COF at (d) room temperature (e) 70 °C, (f) 100 °C.

Table 2 Response, response time, and recovery time for DADE-Tp COF and Zn@DADE-Tp COF at different temperatures for acetylene sensing

Acetylene sensing										
		RT			70 °C			100 °C		
Material	Concentration	Response	T_{res} (s)	T_{rec} (s)	Response	T_{res} (s)	T_{rec} (s)	Response	T_{res} (s)	T_{rec} (s)
DADE-Tp COF	10 ppm	1.03	7.50	7.50	1.03	5.90	4.15	1.05	5.97	5.62
	50 ppm	1.04	5.20	9.50	1.04	5.90	4.29	1.06	7.06	6.58
	100 ppm	1.04	8.93	9.70	1.04	6.98	6.21	1.08	8.42	8.43
	150 ppm	1.04	10.00	10.90	1.05	8.42	7.10	1.08	8.44	8.44
Zn@DADE-Tp COF	10 ppm	1.15	9.23	11.60	1.12	18.66	17.91	1.17	10.00	10.10
	50 ppm	1.20	4.86	5.65	1.18	8.42	8.44	1.22	12.63	12.04
	100 ppm	1.29	14.36	14.78	1.21	15.40	15.40	1.33	14.99	17.63
	150 ppm	1.41	7.32	7.10	1.25	12.31	12.73	1.42	20.66	20.03

more effectively applied for sensing of acetylene gas. It also displays that Zn–COF can be used more effectively for acetylene sensing at room temperature.

4.1 Gas-sensing mechanism

The gas sensing mechanism of a DADE-Tp COF and Zn@DADE-Tp COF sensor involves the adsorption of oxygen on the surfaces of the sensing materials and the interactions of gas molecules adsorbed on these surfaces.[32] Upon exposure of the sensor, to air, oxygen molecules are chemisorbed onto the surface of the detecting material. The oxygen molecules generate chemisorbed oxygen anions (O_2^-, O^- or O^{2-}) by taking electrons from the oxide conduction band. Consequently, an electron depletion layer characterized by a decreased concentration of free electrons develops at the materials surface, thereby, elevating its resistance Fig. 7. The following reaction takes place:

$$O_{2(gas)} \leftrightarrow O_{2(ads)} \quad (2)$$

$$O_{2(ads)} + e \leftrightarrow O_{2(ads)}^- \quad (3)$$

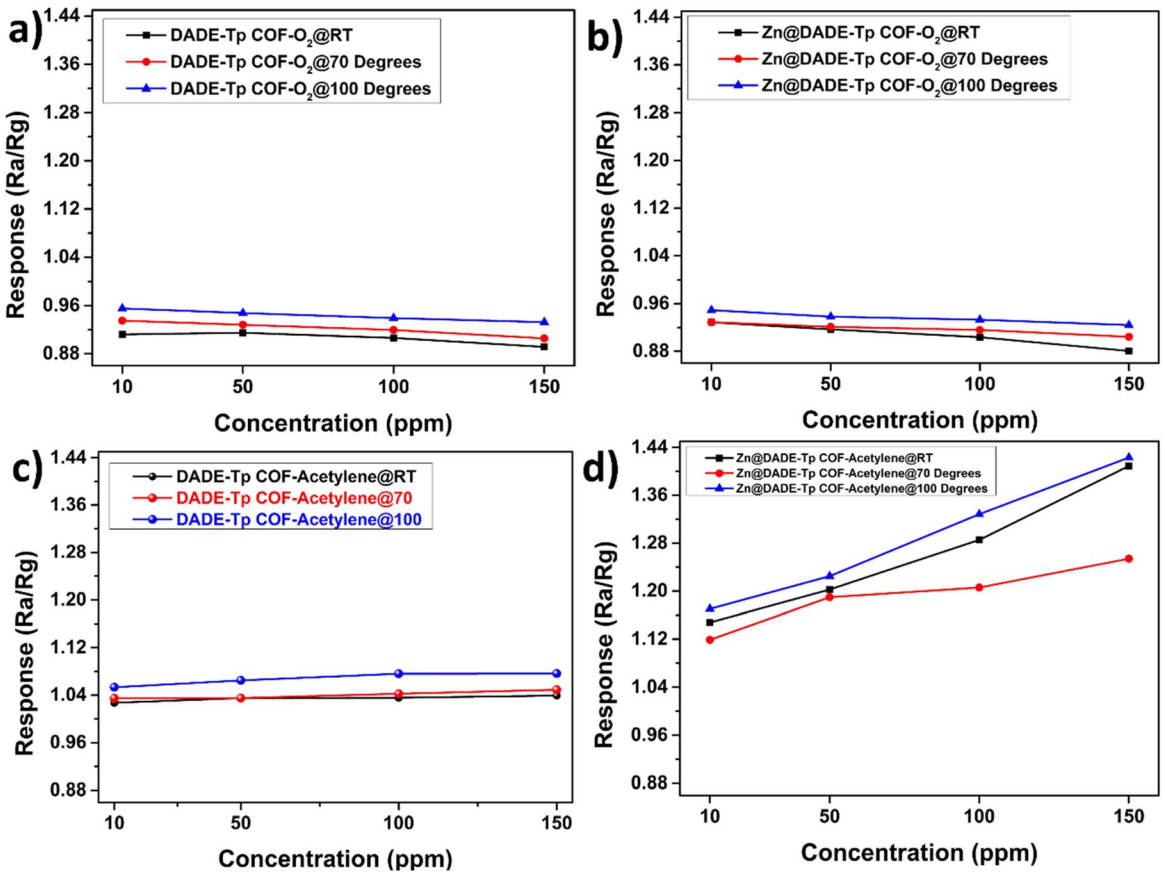

Fig. 5 Response graphs at different concentrations for oxygen sensing by (a) DADE-Tp COF & (b) Zn@DADE-Tp COF, and acetylene sensing by (c) DADE-Tp COF & (d) Zn@DADE-Tp COF.

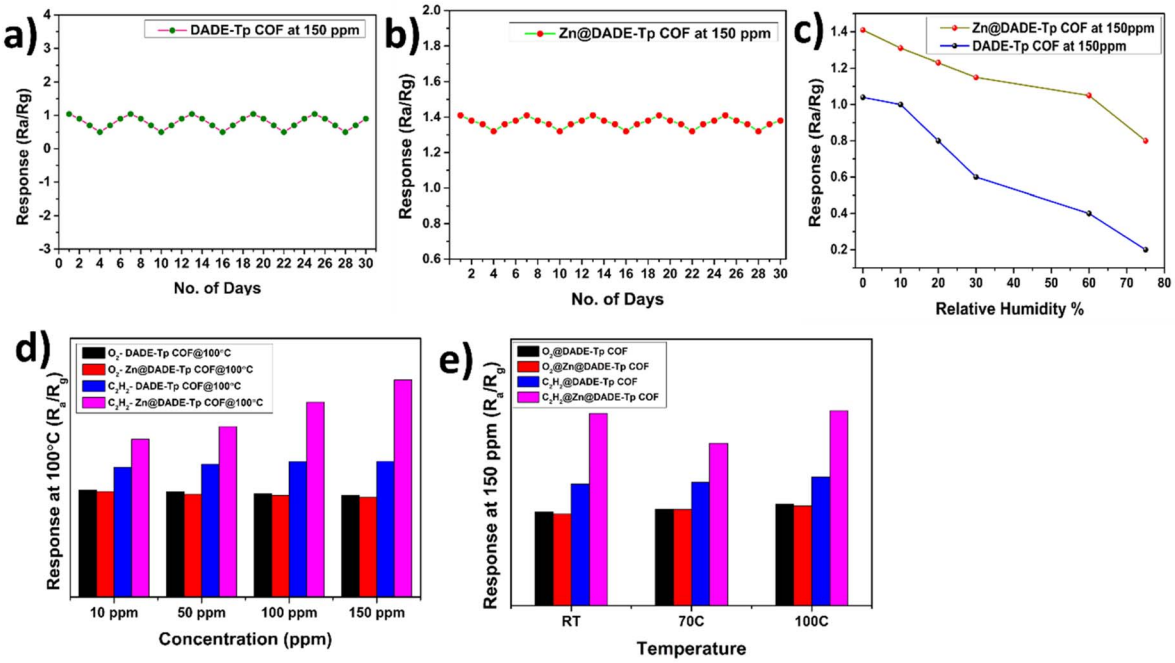

Fig. 6 (a) Stability graph of DADE-Tp COF at 150 ppm, (b) stability graph of Zn@DADE-Tp COF at 150 ppm, (c) relative humidity of DADE-Tp COF and Zn@DADE-Tp COF at 150 ppm, (d) response of DADE-Tp COF and Zn@DADE-Tp COF at 100 °C for all concentrations for oxygen and acetylene sensing (e) response for DADE-Tp COF and Zn@DADE-Tp COF materials at 150 ppm for all the testing temperatures for oxygen and acetylene sensing.

$$O_{2(ads)} + e \leftrightarrow 2O_{(ads)}^{-} \quad (4)$$

$$O_{(ads)}^{-} + 2e^{-} \leftrightarrow O_{ads}^{2-} \quad (5)$$

Upon exposure to acetylene, the DADE-Tp COF and Zn@DADE-Tp COF sensors react with the adsorbed oxygen ions, resulting in the release of electrons back into the conduction band and the formation of a decreased electron depletion barrier. This happens in the following manner:

$$C_2H_2 + 5O_{(ads)}^{-} \rightarrow 2CO_2 + H_2O + 5e^{-} \quad (6)$$

From the above reaction, it can be understood that the electron concentration increases. This, in turn, increases the conductivity of the sensor.[27]

The DADE-Tp COF and Zn@DADE-Tp COF sensors show similar responses, but the Zn@DADE-Tp COF sensor showed a larger change in resistance, thus reducing the response time. This sensor shows a very good response and recovery time for acetylene sensing at room temperature when compared to the others, which were good at higher temperatures. It can also detect acetylene at a concentration as low as 10 ppm. Table 3 shows the comparison of our work with other sensors.

To support the experimentally observed superior sensing response of Zn@DADE-Tp COF towards acetylene (C_2H_2),

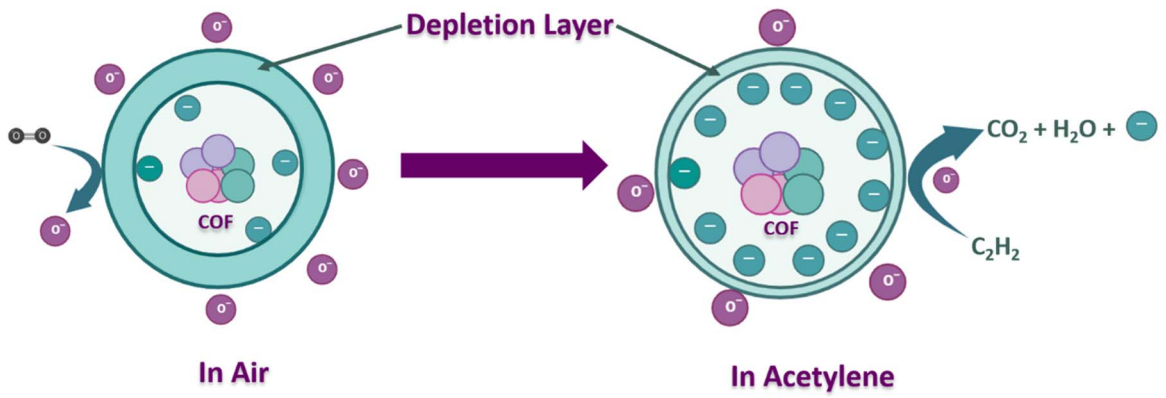

Fig. 7 Schematic illustration of the gas sensing mechanism.

Table 3 Comparison table of the acetylene sensing present work with previous works

Material	Gas concentration (ppm)	Response ($S = R_a/R_g$)	Operating temperatures	T_{res}	T_{rec}	Ref.
Pt/ZnO	50–10000	836 (10 000 ppm) 43 (1000 ppm)	300 °C	6	65	33
Ni–ZnO	100–2000	17 (2000 ppm)	250 °C	5	10	34
ZnO	1–4000	52 (200 ppm)	420 °C	15	19	35
ZnO/rGO	30–1000	18.2 (100 ppm)	250 °C	100	28	36
CuO/ZnO		7.6 (10 ppm)	200 °C			37
COF	10–150	1.04 (150 ppm)	RT	10.00	10.90	Present work
Zn–COF	10–150	1.41 (150 ppm)	RT	7.32	7.1	Present work

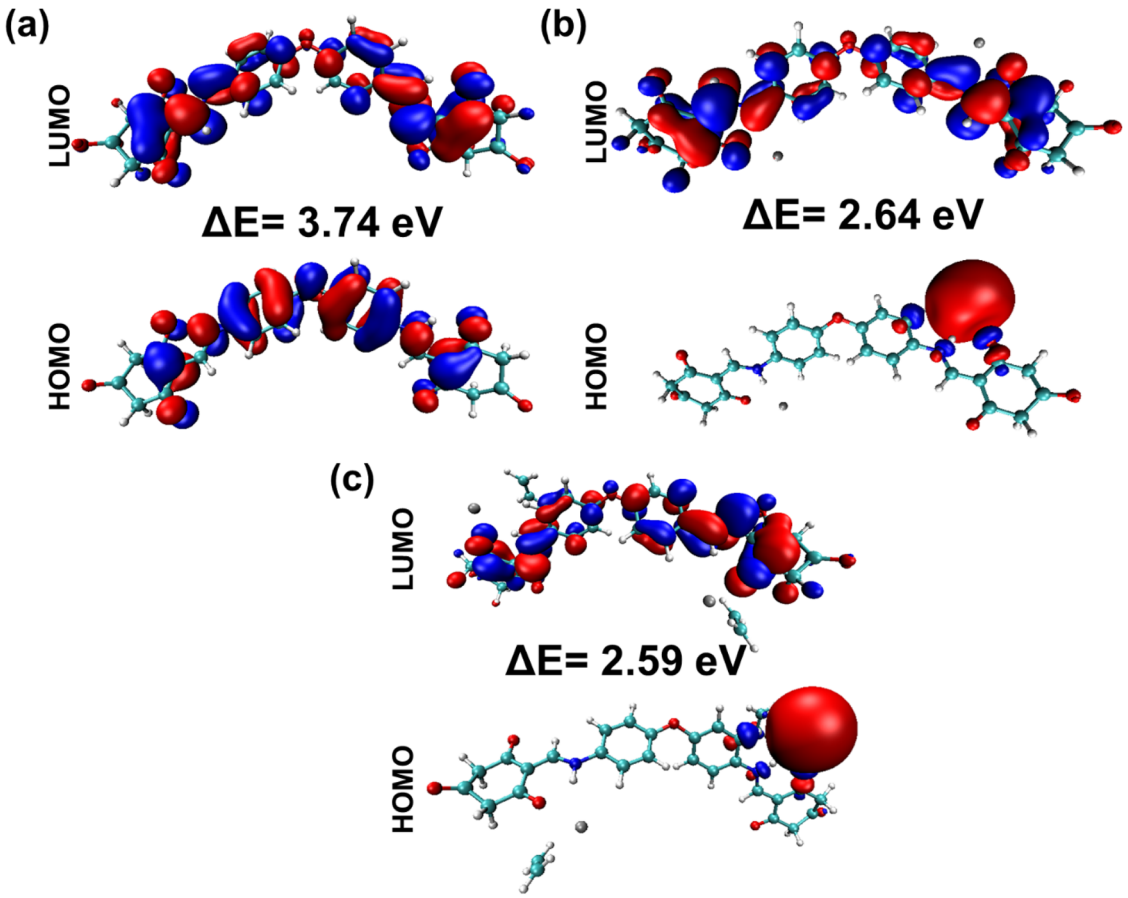

Fig. 8 HOMO and LUMO plots of COFs rendered at an isosurface value of 0.02 a.u. (a) DADE-Tp COF, (b) Zn@DADE-Tp COF, and (c) Zn@DADE-Tp–C_2H_2.

detailed density functional theory (DFT) calculations were performed. These included an analysis of the electronic structure (HOMO–LUMO gap), frontier molecular orbitals, and electrostatic potential (ESP) graphs for the pristine DADE-Tp COF, Zn@DADE-Tp COF, and the Zn@DADE-Tp-C_2H_2 complex.

The HOMO–LUMO energy gap is a key factor in the electronic properties of sensing materials. As summarized in Table S3† and Fig. 8a–c, the pristine DADE-Tp COF exhibits a wide energy gap of 3.74 eV, signifying limited intrinsic conductivity. Upon Zn@DADE-Tp COF, the energy gap reduces to 2.64 eV, which indicates enhanced electronic delocalization and improved charge carrier mobility. This reduction in energy gap plays a critical role in facilitating electron transfer during gas sensing analysis. Notably, after the adsorption of C_2H_2 on Zn@DADE-Tp COF, the energy gap further decreases to 2.59 eV, confirming that strong interactions occur between the Zn@DADE-Tp COF and the active sites of the framework. The frontier molecular orbital plots, Fig. 8a–c, provide further insight into the sensing mechanism. In the pristine COF, the HOMO and LUMO orbitals are primarily localized over isolated units, suggesting restricted electron mobility. Upon Zn incorporation, these orbitals become more delocalized across the conjugated framework, especially around the Zn coordination center, thereby facilitating faster charge transport. Upon C_2H_2 adsorption, the orbital distribution becomes significantly polarized at the binding site, indicating strong interaction and

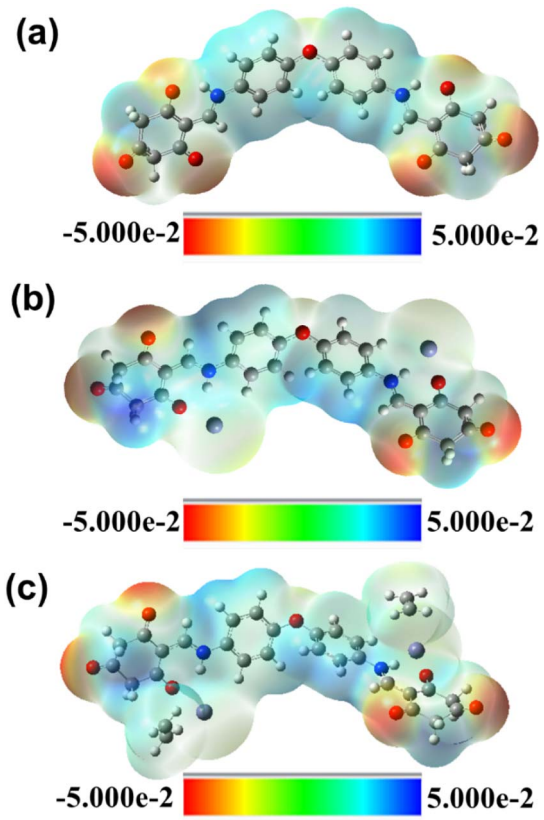

Fig. 9 Electrostatic potential graphs of COFs (a) DADE-Tp COF, (b) Zn@DADE-Tp COF, and (c) Zn@DADE-Tp – C_2H_2.

potential for efficient charge transfer during the sensing process. Electrostatic potential (ESP) images (Fig. 9a–c) further validate the observed changes in electronic distribution. The pristine DADE-Tp COF shows a relatively uniform ESP surface, while Zn@DADE-Tp COF exhibits enhanced charge separation with localized negative regions near electronegative atoms and Zn centers. After C_2H_2 adsorption, the ESP graph becomes more perturbed, particularly around the adsorption site, signifying strong electrostatic interactions. These interactions help in stabilizing the gas molecule on the surface and facilitating charge redistribution, which is reflected in the observed decrease in energy gap.

In summary, the combined theoretical analyses encompass the progressive reduction in HOMO–LUMO energy gap. Enhanced delocalization of frontier molecular orbitals and intensified electrostatic potential around the Zn coordination site corroborate the experimentally observed enhancement in the acetylene sensing performance of Zn@DADE-Tp COF. The incorporation of Zn not only modulates the electronic structure by decreasing the energy gap and facilitating charge carrier mobility but also introduces chemically active sites that enable strong interaction with C_2H_2 molecules. Collectively, these findings provide a comprehensive theoretical rationale for the role of Zn as a functional dopant in tailoring the electronic and sensing properties of COF-based materials for selective acetylene detection.

5 Conclusion

This study illustrates the effective design of a Zn^{2+}-doped covalent organic framework (Zn@DADE-Tp COF) that attains remarkable room-temperature acetylene sensing capabilities, featuring rapid response/recovery times (7.32 s/7.10 s), outstanding sensitivity (1.41 response at 150 ppm), and minimal detection limits (10 ppm), exceeding traditional metal-oxide sensors. Comprehensive characterization (PXRD, XPS, TEM, AFM) demonstrated that Zn^{2+} incorporation generates optimal Lewis-acidic sites for selective acetylene binding while preserving structural integrity, with a surface roughness of 137.32 nm and π-conjugated frameworks facilitating efficient charge transport. The material's durability (below 250 °C) and selectivity in humid conditions render it a viable choice for industrial safety monitoring in welding, power transformers, and lithium battery manufacturing. This research enhances COF-based sensor design and offers a comprehensive method for the engineering of metal-coordinated porous materials, with subsequent efforts aimed at scalable synthesis and integration with IoT systems for real-time leak detection. By integrating fundamental materials chemistry with applied sensor technology, Zn@DADE-Tp COF signifies a substantial advancement in energy-efficient, next-generation gas detection devices.

Ethical statement

This article does not contain any studies with animals performed by any of the authors.

Consent for publication

We authorize to publish the article without any conflict.

Data availability

All data generated or analyzed during this study are included in this published article and its ESI files.†

Author contributions

Ms. Prerana Loomba: Investigation, methodology, formal analysis and writing – original draft. Mr. Sujith Benarzee Nallamalla: Formal analysis and writing – original draft. Dr Kopulla Suresh: Data curation, and software. Dr Naresh Kumar Katari: Visualisation, and resources. Prof. Surendra Babu Manabolu Surya: Conceptualisation, validation, project administration, supervision, and writing-review & editing.

Conflicts of interest

The authors declare no conflict of interest regarding the publication of this manuscript.

Acknowledgements

The authors acknowledge CIF, GITAM deemed to be a University, for the facilities and SAIF, NMR facility at IISC Bangalore, for providing solid state NMR spectra. Author S. B. N. thanks DST, INDIA, for financial support for the INSPIRE fellowship (INSPIRE Code: IF210570).

References

1 M. S. Park, J. H. Lee, Y. Park, R. Yoo, S. Park, H. Jung, W. Kim, H. S. Lee and W. Lee, *Sens. Actuators, B*, 2019, **299**, 126992, DOI: 10.1016/j.snb.2019.126992.
2 K. Wan, D. Wang, F. Wang, H. Li, J. Xu, X. Wang and J. Yang, *ACS Appl. Mater. Interfaces*, 2019, **11**, 45214–45225, DOI: 10.1021/acsami.9b16599.
3 S. C. L and J. N. Chandra Sekhar, *J. Mod. Technol.*, 2025, **02**, 254–263, DOI: 10.71426/jmt.v2.i1.pp254-263.
4 N. R. Williams and R. M. Whittington, *J. Toxicol., Clin. Toxicol.*, 2001, **39**, 69–71, DOI: 10.1081/clt-100102882.
5 C. Jiang, D. Zhang, N. Yin, Y. Yao, T. Shaymurat and X. Zhou, *Nanomaterials*, 2017, **7**, 278, DOI: 10.3390/nano7090278.
6 A. Milone, A. G. Monteduro, S. Rizzato, A. Leo, C. Di Natale, S. S. Kim and G. Maruccio, *Adv. Sustainable Syst.*, 2023, **7**, 2200083, DOI: 10.1002/adsu.202200083.
7 H. J. Kim and J. H. Lee, *Sens. Actuators, B*, 2014, **192**, 607–627, DOI: 10.1016/j.snb.2013.11.005.
8 X. Zhang, G. Li, D. Wu, B. Zhang, N. Hu, H. Wang, J. Liu and Y. Wu, *Biosens. Bioelectron.*, 2019, **145**, 111699, DOI: 10.1016/j.bios.2019.111699.
9 P. J. Waller, F. Gándara and O. M. Yaghi, *Acc. Chem. Res.*, 2015, **48**, 3053–3063, DOI: 10.1021/acs.accounts.5b00369.
10 Z. Meng and K. A. Mirica, *Chem. Soc. Rev.*, 2021, **50**, 13498, DOI: 10.1039/d1cs00600b.
11 X. Liu, D. Huang, C. Lai, G. Zeng, L. Qin, H. Wang, H. Yi, B. Li, S. Liu, M. Zhang, R. Deng, Y. Fu, L. Li, W. Xue and S. Chen, *Chem. Soc. Rev.*, 2019, **48**, 5266–5302, DOI: 10.1039/c9cs00299e.
12 M. Wang, M. Wang, H. H. Lin, M. Ballabio, H. Zhong, M. Bonn, S. Zhou, T. Heine, E. Cánovas, R. Dong and X. Feng, *J. Am. Chem. Soc.*, 2020, **142**, 21622–21627, DOI: 10.1021/jacs.0c10482.
13 E. Martínez-periñán, M. Martínez-fernández, J. L. Segura and E. Lorenzo, *Sensors*, 2022, **22**, 4758, DOI: 10.3390/s22134758.
14 S. Kandambeth, A. Mallick, B. Lukose, M. V. Mane, T. Heine and R. Banerjee, *J. Am. Chem. Soc.*, 2012, **134**, 19524–19527, DOI: 10.1021/ja308278w.
15 S. Kandambeth, B. P. Biswal, H. D. Chaudhari, K. C. Rout, S. Kunjattu H, S. Mitra, S. Karak, A. Das, R. Mukherjee, U. K. Kharul and R. Banerjee, *Adv. Mater.*, 2017, **29**, 1603945, DOI: 10.1002/adma.201603945.
16 D. Zhu and R. Verduzco, *ACS Appl. Mater. Interfaces*, 2020, **12**(29), 33121–33127, DOI: 10.1021/acsami.0c09173.
17 Y. J Dibdalli, C. Morales-Verdejo, D. E. Ortega, E. Molins and M. K. Amshumali, *J. Mol. Struct.*, 2024, **1309**, 138163, DOI: 10.1016/j.molstruc.2024.138163.
18 E. Torres and G. A. Dilabio, *J. Phys. Chem. Lett.*, 2012, **3**, 1738–1744, DOI: 10.1021/jz300554y.
19 S. B. Nallamalla, N. K. Katari, A. J. M. Reddy, S. B. Jonnalagadda and S. B. Manabolu Surya, *RSC Adv.*, 2025, **15**, 16708–16723, DOI: 10.1039/D5RA01430A.
20 K. Koner, S. Mohata, Y. Ogaeri, Y. Nishiyama, M. A. Addicoat and R. Banerjee, *Angew. Chem., Int. Ed.*, 2024, **63**, e202316873, DOI: 10.1002/anie.202316873.
21 F. Haase and B. V. Lotsch, *Chem. Soc. Rev.*, 2020, **49**, 8469–8500, DOI: 10.1039/d0cs01027h.
22 K. Dey, M. Pal, K. C. Rout, S. Kunjattu H, A. Das, R. Mukherjee, U. K. Kharul and R. Banerjee, *J. Am. Chem. Soc.*, 2017, **139**, 13083–13091, DOI: 10.1021/jacs.7b06640.
23 Q. Cao, L. L. Zhang, C. Zhou, J. H. He, A. Marcomini and J. M. Lu, *Appl. Catal., B*, 2021, **294**, 120238, DOI: 10.1016/j.apcatb.2021.120238.
24 T. Yu, W. Su, W. Li, Z. Hong, R. Hua, M. Li, B. Chu, B. Li, Z. Zhang and Z. Z. Hu, *Inorg. Chim. Acta*, 2006, **359**, 2246–2251, DOI: 10.1016/j.ica.2006.01.019.
25 J. Wang, H. Li, S. Liu, Y. Hu, J. Zhang, M. Xia, Y. Hou, J. Tse, J. Zhang and Y. Zhao, *Angew. Chem., Int. Ed.*, 2021, **133**, 183–187, DOI: 10.1002/ange.202009991.
26 S. Ghosh, R. A. Molla, U. Kayal, A. Bhaumik and S. M. Islam, *Dalton Trans.*, 2019, **48**, 4657–4666, DOI: 10.1039/C9DT00017H.
27 B. Shouli, C. Liangyuan, L. Dianqing, Y. Wensheng, Y. Pengcheng, L. Zhiyong, C. Aifan and C. C. Liu, *Sens. Actuators, B*, 2010, **146**, 129–137, DOI: 10.1016/j.snb.2010.02.011.
28 S. Park, P. M. Bulemo, W. T. Koo, J. Ko and I. D. Kim, *Sens. Actuators, B*, 2021, **343**, 130137, DOI: 10.1016/j.snb.2021.130137.
29 F. Liu and Z. Fan, *Chem. Soc. Rev.*, 2023, **52**, 1723–1772, DOI: 10.1039/D2CS00931E.
30 Y. Yang, L. Ge, V. Rudolph and Z. Zhu, *Dalton Trans.*, 2014, **43**, 7028–7036, DOI: 10.1039/C3DT53191K.
31 Y. V. Kaneti, S. Dutta, M. S. A. Hossain, M. J. A. Shiddiky, K. L. Tung, F. K. Shieh, C. K. Tsung, K. C. W. Wu and Y. Yamauchi, *Adv. Mater.*, 2017, **29**, 1700213, DOI: 10.1002/adma.201700213.
32 R. Thayil and S. R. Parne, *J. Mater. Sci.: Mater. Electron.*, 2025, **36**, 322, DOI: 10.1007/s10854-025-14401-1.
33 N. Tamaekong, C. Liewhiran, A. Wisitsoraat and S. Phanichphant, *Sens. Actuators, B*, 2011, **152**, 155–161, DOI: 10.1016/j.snb.2010.11.058.
34 X. Wang, M. Zhao, F. Liu, J. Jia, X. Li and L. Cao, *Ceram. Int.*, 2013, **39**, 2883–2887, DOI: 10.1016/j.ceramint.2012.09.062.
35 L. Zhang, J. Zhao, J. Zheng, L. Li and Z. Zhu, *Sens. Actuators, B*, 2011, **158**, 144–150, DOI: 10.1016/j.snb.2011.05.057.
36 A. S. M. I. Uddin and G. S. Chung, *Sens. Actuators, B*, 2014, **205**, 338–344, DOI: 10.1016/j.snb.2014.09.005.
37 M. H. Jung, M. Kwak, J. Ahn, J. Y. Song, H. Kang and H. T. Jung, *ACS Sens.*, 2024, **9**, 217–227, DOI: 10.1021/acssensors.3c01844.